Materials Chemistry and Physics 213 (2018) 267–276

Contents lists available at ScienceDirect

Materials Chemistry and Physics

journal homepage: www.elsevier.com/locate/matchemphys

A novel porous carbon material made from wild rice stem and its application in supercapacitors

Qiang Tian [a], Xiaoxue Wang [a], Xiaoyang Xu [c], Man Zhang [a], Luyao Wang [a], Xiaoxiang Zhao [a], Zhaolin An [a], Hongduo Yao [a], Jianping Gao [a, b, *]

[a] Department of Chemistry, School of Science, Tianjin University, Tianjin 300350, China
[b] Collaborative Innovation Center of Chemical Science and Engineering (Tianjin), Tianjin 300072, China
[c] Department of Chemistry, School of Science, Hebei University of Science and Technology, Hebei 050000, China

HIGHLIGHTS

- Wild rice stem was converted into activated porous carbon for electrode materials.
- The porous carbon possesses high specific surface area and abundant pore distribution.
- The highest specific capacitance of activated porous carbon is as high as 301 F/g at current density of 1 A/g.
- The supercapacitor exhibits excellent rate performance and cycling stability.

GRAPHICAL ABSTRACT

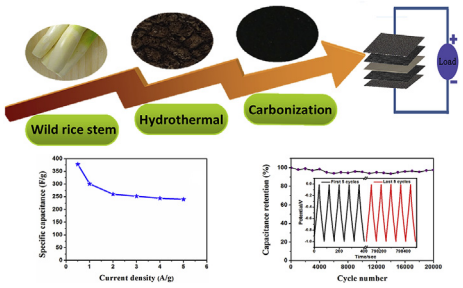

ARTICLE INFO

Article history:
Received 6 September 2017
Received in revised form
24 January 2018
Accepted 7 April 2018
Available online 9 April 2018

Keywords:
Wild rice stem
Activated porous carbon
Electrode materials
Supercapacitor

ABSTRACT

Nowadays, it is known that activated porous carbon materials behave high specific capacitance owing to their high specific surface area, microporous and mesoporous structures. Therefore, the carbon materials with low cost and good cycle stability become one of the most promising electrode materials in supercapacitors. In this paper, the carbon material prepared by the carbonization of wild rice stem and the alkali activation possesses high specific surface area up to 1228 m^2/g, which makes it more hopeful application prospects in electrochemical field. The results indicate that activation temperature and alkali concentration play important roles in improving the performance of specific capacitance of the activated carbon. The activated porous carbon prepared at 800 °C with a KOH/wild rice stem mass ratio of 3 shows the best performance and displays a specific capacitance of 301 F/g at current density of 1 A/g in a three-electrode configuration. Furthermore, the assembled symmetric supercapacitor attains a high energy density of 13.05 Wh/kg at the power density of 250 W/kg in 6 M KOH electrolyte. So the activated porous carbon made from wild rice stem is a low-cost, eco-friendly and high performance material for supercapacitors.

1. Introduction

With the fossil fuel resource lack and the problem of air pollution being very serious, scientists are enforced to look for a new eco-friendly energy storage device to solve this tricky question

* Corresponding author. Department of Chemistry, School of Science, Tianjin University, Tianjin 300350, China.
E-mail address: jianpinggaols@126.com (J. Gao).

https://doi.org/10.1016/j.matchemphys.2018.04.026
0254-0584/

[1–4]. Owing to their superior performance of high power density, short charging time, long cycle life, good temperature characteristics and better operation safety, supercapacitors are becoming a critical device for energy storage that can replace some of the traditional chemical batteries [5–9]. Supercapacitors are also called electrochemical capacitors which consist of electric double layer capacitors (EDLCs) and pseudo-capacitors. The EDLCs act as an energy storage device by adsorbing the ions of electrolyte at the electrolyte/electrode interface [10]. They are firstly commercialized due to their excellent performance and long cycle life. In general, the electrodes of EDLCs are carbon-based materials such as activated carbons (ACs), activated carbon fiber, charcoal gels, carbon nanotubes and graphene, of which ACs are the most widely used electrode materials due to their large surface area and good electrochemical properties [11].

Recently, bio-derived activated porous carbon materials are widely applied to electrode materials for supercapacitors and have attracted much attention because of low production costs and abundant sources. Activated porous carbons can be easily produced by carbonization and activation of natural biomass. However, the types of biomass and activator and carbonization temperature significantly influence electrochemical performance of the as-prepared carbon materials. Thus it is necessary to carry out continuous studies to obtain the best carbon materials [12,13]. Much work so far has focused on the choice of activators, such as potassium hydroxide, sodium hydroxide, phosphoric acid or zinc chloride, etc. [14]. Favorable activator can effectively improve pore volume and the specific surface area of carbon materials. Nevertheless, the high specific surface area is not the only factor determining the electrochemical performance of the materials. The distribution, shape and structure of pores, as well as functional modification of materials also affect the electrochemical properties of the activated porous carbons [15,16]. Therefore, the design of activated carbon materials with narrow pore size distribution, cross-linked pore structure, short ion transport distances and controlled surface chemical properties will help to increase the energy density of supercapacitors without compromising power density and cycle life.

At present, biomass materials can be used to prepare porous carbon materials that display good capacitance performance [17–25]. The carbon materials from almond shell and paulownia flower show high specific capacitances of 272.3 F/g and 297 F/g at the current density of 1 A/g [21,26]. Momodu used tree bark to prepare a carbon material that has a specific surface area of 1018 m^2/g and shows a specific capacitance of 191 F/g at current density of 1 A/g [27]. Therefore, developing carbon materials from biomass for supercapacitors is a useful and promising approach.

Here, wild rice stem is used as biomass precursor for the preparation of activated porous carbon by the carbonization and activation processes. It is commonly known that the wild rice stem belongs to herb of marsh of gramineous vivacious perennial root and has a wide range of food and medicinal values. In this paper, the wild rice stem was firstly subjected to hydrothermal treatment. Afterwards, the porous carbon material with oxygen-enriched functional groups was obtained by twice carbonation and activation with the mass ratio of KOH to material of 3:1. The resulting activated wild rice stem carbon (A-WRSC) showed a high specific capacitance of 301 F/g at current density of 1 A/g. The symmetric supercapacitor based on A-WRSC electrodes achieved a high energy density of 13.05 Wh/kg at the power density of 250 W/kg. Thus, the wild rice stem possesses excellent application prospects for the preparation of carbon electrode materials.

2. Experimental section

2.1. Materials

All reagents used in the experiment were analytical grade and without further purification. Potassium hydroxide (KOH) and hydrochloric acid (HCl) were obtained from Tianjin Chemical Reagent Company. The fresh wild rice stem was purchased from Carrefour supermarket.

2.2. Preparation of the A-WRSC materials

The white fleshy part of the wild rice stem was chosen to make A-WRSC. It was firstly peeled and cut into small pieces, washed with deionized water, and then it was freeze-dried for 24 h under the condition of vacuum. The dried sample (1 g) was dispersed into 45 mL distilled water and stirred for 1 h. The dispersion was then put into a 100 ml Teflon-lined stainless autoclave for hydrothermal treatment at 180 °C for 18 h. After cooling to room temperature, the resultant product was subjected to pyrolysis at 500 °C for 3 h in nitrogen atmosphere. Subsequently, the obtained product was mixed with a certain concentration of KOH solution (A large number of repetitive experiments proved that the ratio of KOH to sample of 3:1 obtained the best activation effect). After mixing evenly, the mixture was dried at 120 °C for 12 h and then calcined at 700 °C (800 °C or 900 °C) for 2 h under the atmosphere of inert gas. The resulting carbon material was washed with HCl solution (1 M) and deionized water several times until the supernatant was neutral (pH = 7). At last, the carbon material was dried at 100 °C in drying oven for 12 h (Fig. 1). The A-WRSC sample prepared at activation temperature B was denoted as A-WRSC-B. As a control, the sample without KOH activation is denoted as WRSC.

2.3. Characterizations of the A-WRSC materials

The surface morphology of A-WRSC materials was characterized by scanning electron microscopy (SEM, Hitachi S-4800 microscope operated at 3.0 kV) and transmission electron microscopy (TEM, Philips Tecnai G2F20 microscope operated at 200 kV). X-ray powder diffraction (XRD, BDX3300) and Raman spectroscopy (DXR Microscope, USA) were used to analyze graphitization degree and crystallization situations of the A-WRSC. Elemental composition and functional groups of the A-WRSC were determined by X-ray photoelectron spectroscopy (XPS, PHI1600 ESCA System, US, operated with an Mg Ka anode) and Fourier transform infrared spectroscopy (FT-IR, Nicolet 6700). The surface area and pore structure of the as-prepared A-WRSC were characterized by the N2 sorption tests at 77.35 K (The pressure of the degas step is 100 μm mercury column). Specific surface area was calculated using the

Fig. 1. Schematic illustration of A-WRSC preparation.

Brunauer-Emmett-Teller (BET) equation, whereas the pore size distribution was obtained by the BJH (Barrett, Joyner, Halender) method.

2.4. Electrochemical measurements of the A-WRSC electrodes

The electrochemical tests were carried out by using an electrochemical workstation (CHI 660) under computer control, which includes cyclic voltammetry (CV), galvanostatic charge–discharge (GCD) and electrochemical impedance spectroscopy (EIS) in the two or three-electrode systems. In the three-electrode system, working electrode was fabricated by mixing activated material (~4 mg), carbon black and polytetrafluoroethylene emulsion with the mass ratio of 75:15:10 to result in working electrode paste that was then smeared on the nickel foam (1×1 cm^2). In the three-electrode system, 6 mol/L potassium hydroxide electrolyte solution was applied as electrolyte, Pt mesh served as the auxiliary electrode, and the Hg/HgO electrode was used as the reference electrode. The specific capacitance (Cs) of the electrode was calculated using the following equation:

$$Cs = \frac{i \times \Delta t}{m \times \Delta v} \quad (1)$$

where i is the current (A), Δt is the discharge time (s), Δv is the potential window (V) and m is the mass of the active material (g).

The symmetric two-electrode system was assembled using two identical working electrode plates as the positive and negative electrodes (each electrode has a mass of 4 mg) in the 6 M KOH electrolyte, separated by a 0.18 μm thick microfiber glass filter paper. The specific capacitances, energy density, and power density of the devices were determined using the equations:

$$C = \frac{I \times \Delta t}{M \times \Delta U} \quad (2)$$

$$E = \frac{1}{2} C(\Delta U)^2 \quad (3)$$

$$P = \frac{E}{\Delta t} \quad (4)$$

where C is total specific capacitance (F/g), I is the discharge current (A), Δt is the discharge time (s), M is the total mass of the active material on both electrodes (g), ΔU is the voltage window (V), E is the energy density (Wh/kg), and P is the power density (W/kg).

3. Results and discussion

3.1. Surface morphology and porous structure of A-WRSC

It is generally believed that high specific surface area with abundant pore size distribution is of great importance for capacitance performance of carbon material electrodes [28]. Here, the surface morphology and pore formation of the A-WRSC are analyzed by scanning electron microscopy (SEM) and transmission electron microscopy (TEM). The SEM images of WRSC in Fig. 2a–b obviously display large blocks structure with messy stacked phenomenon. Whereas, after alkali activation, the activated A-WRSC has smaller size compared with WRSC and displays macroporous structure owing to the aggregation of the particles (Fig. 2c–d). So alkali activation can successfully improve the pore volume of the carbon made from wild rice stem.

The representative TEM images of A-WRSC-800 are reflected in Fig. 2e–h. It clearly demonstrates mesoporous structure indicated by the light and dark regions in the image. The mesoporous structure is beneficial to the effective contact between the electrolyte ions and the electrode material. In the high-resolution TEM images, no lattice stripes are found, manifesting the sample is amorphous.

To gain more insight of the surface structure and pore size distribution of the A-WRSC, the nitrogen adsorption and desorption isotherms are shown in Fig. 3a. All the samples show similar profiles which are in good agreement with the I/IV-type adsorption-desorption isotherm. In the low relative pressure region ($P/P_0 < 0.1$), the gas adsorption capacities have a rapid growth, which suggests that the samples possess rich microporous structure. In addition, there are visible hysteresis loops in the high relative pressure area ($P/P_0 > 0.3$), explaining the presence of mesoporous adsorption. Among the three samples, A-WRSC-800 attains the highest specific surface area of 1228 m^2/g with a specific pore volume of 0.557 cm^3/g.

The pore size distributions (PSD) of the samples are shown in Fig. 3b. It is found that the pores have a wide distribution in the range of 0.57–1.4 nm, which indicates the presence of a large number of micropores and moderate mesopores [29,30]. This is consistent with the observation from TEM images. Furthermore, the sample of A-WRSC-800 exhibits larger pores volume than other A-WRSC samples, resulting in a higher specific surface area. The formation mechanism of pores can be summarized as follows:

$$6KOH + C \rightarrow 2K + 3H_2 + 2K_2CO_3 \quad (5)$$

$$K_2CO_3 \rightarrow K_2O + CO_2 \quad (6)$$

$$K_2CO_3 + 2HCl \rightarrow 2KCl + H_2O + CO_2 \quad (7)$$

$$K_2O + 2HCl \rightarrow 2KCl + H_2O \quad (8)$$

Thus, with the reaction of carbon and potassium hydroxide at high temperature, K_2CO_3, K_2O and metal potassium intermediates are produced [31–33]. After further washing with HCl solution and distilled water, they are dissolved and leave pores. Meanwhile, the resulting water at high temperature and carbon dioxide may also create more pores.

3.2. Crystal structure and surface functional group analysis

Fig. 4a shows the XRD patterns of the A-WRSC samples. It is worthwhile to mention that all the samples display two diffraction peaks at 20.5° and 43.1° that correspond to (002) and (100) graphitic planes, respectively. The appearance of two broad and weak diffraction peaks illustrates the samples include some amorphous carbon [34,35]. In addition, the intensity of XRD peaks increases with the annealing temperature, which indicates the enhanced crystallinity of the samples. The crystal structure of the A-WRSC-800 can be further analyzed by Raman spectroscopy. As can be seen from Fig. 4b, A-WRSC-800 shows two bands at 1340 cm^{-1} and 1587 cm^{-1} which are in good agreement with D band and G band. The D band and G band are related to the lattice disorder and the vibration of sp^2 hybridized carbon atom, respectively [36]. The intensity ratio of D band and G band (ID/IG) of sample A-WRSC-800 illustrates the appropriate degree of graphitization after high temperature activation process [25].

TGA is a thermal analysis technique that measures the relationship between the mass and the temperature, so as to study the thermal stability and composition of the materials. The TGA profiles of A-WRSC-700, A-WRSC-800 and A-WRSC-900 (Fig. 4c) exhibit initial weight loss of around 5, 8 and 8% below 100 °C as a result of evaporation of the physically adsorbed water molecules [24]. In

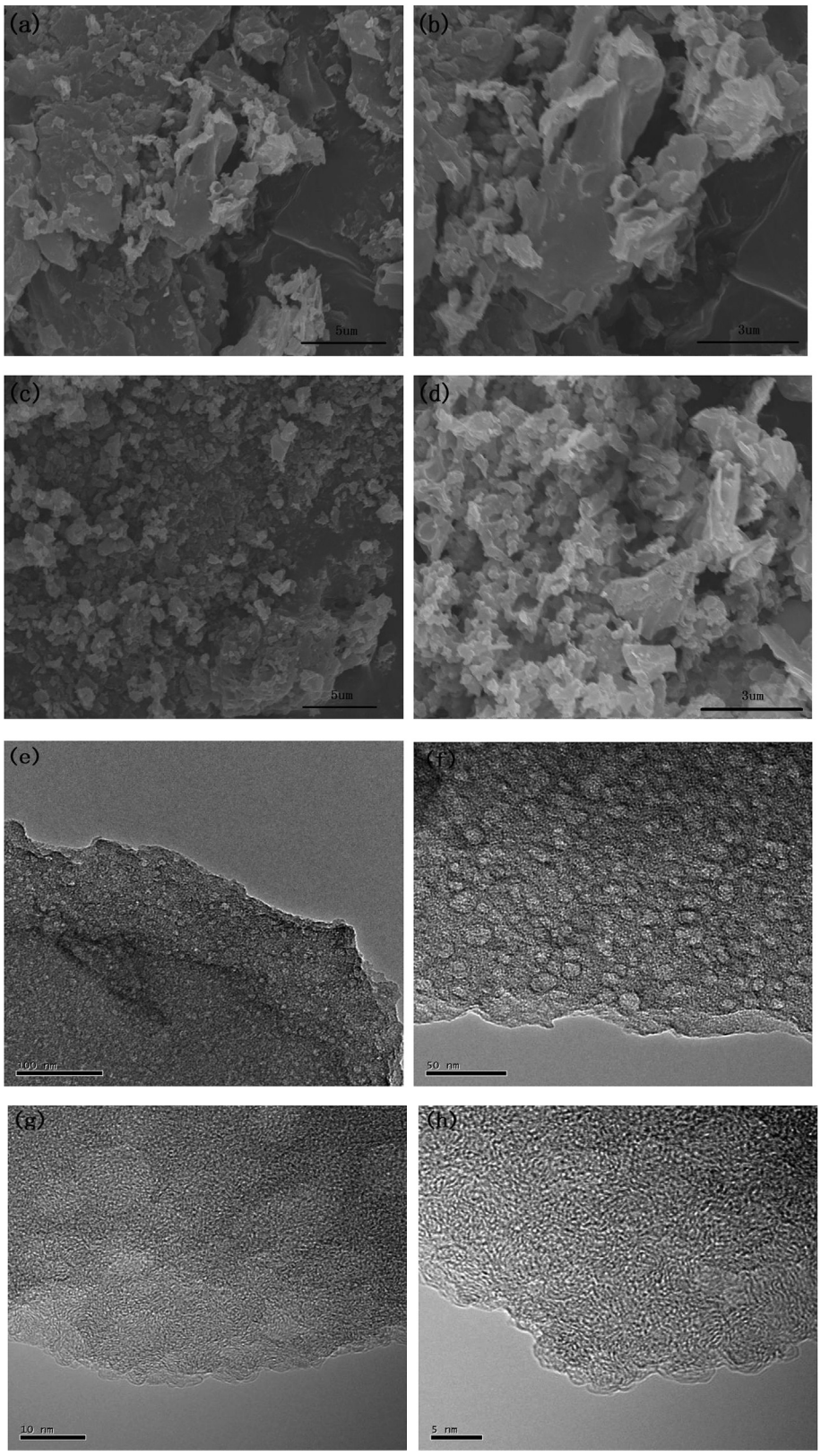

Fig. 2. SEM images of WRSC-800 (a, b) and A-WRSC-800 (c, d); TEM images of A-WRSC-800 (e, f) and high-resolution TEM images of A-WRSC-800 (g, h).

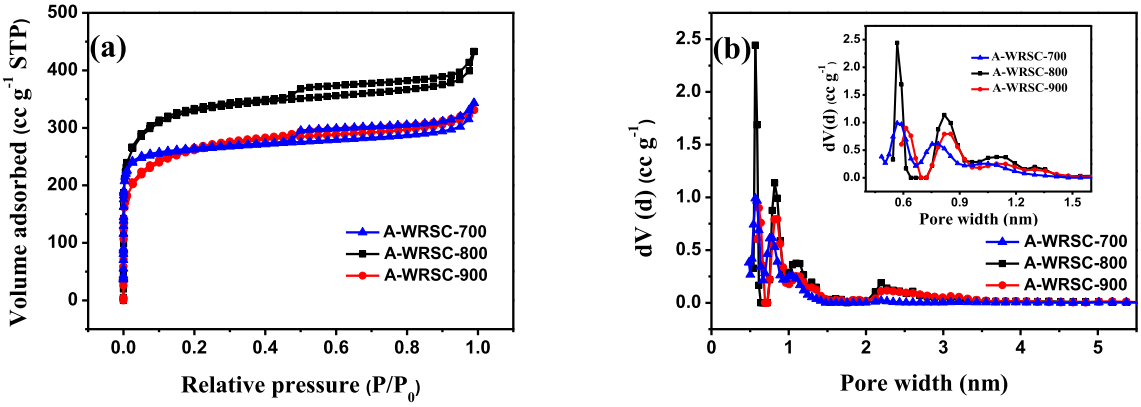

Fig. 3. Nitrogen gas adsorption-desorption profile (a) and pore size distribution (b) of A-WRSC-700, A-WRSC-800 and A-WRSC-900.

addition, the sample A-WRSC-700 shows a drastic weight loss of 100% between 400 and 520 °C due to the complete decomposition of carbon in the air. Whereas, the sample of A-WRSC-800 and A-WRSC-900 exhibited the complete decomposition profiles at slightly high temperature range (400–560 °C, 400–600 °C), indicating the presence of higher degree of graphitization and more stable carbon. Above 600 °C, the decomposition profiles display 100% weight loss, so it is confirmed that the samples contain only carbon and there is no other metal/metal oxide impurities.

In order to understand the chemical structure of the samples, the IR spectra of A-WRSC-700, A-WRSC-800 and A-WRSC-900 are shown in Fig. 4d. The three samples (~1 mg) all indicate the existence of oxygen-containing functional groups [37]. It is clearly identified that broad peak at 3434 cm^{-1} refers to O-H stretching and the small peak at 1175 cm^{-1} is assigned to C-O stretching. Moreover, the sharp peaks at 2989 cm^{-1}, 1629 cm^{-1} and 1398 cm^{-1} are attributed to C-H stretching, C=C stretching and C-H asymmetrical bending, respectively. The IR spectra curves display that the peak intensity of functional groups of the sample are gradually decreased by rising the activation temperature, because high activation temperature may result in increased degree of graphitization.

XPS is a useful analytical tool to study the elemental composition and molecular structure of compounds. XPS spectrum of sample A-WRSC-800 in Fig. 4e shows two distinct peaks in the binding energy at 284.5 and 533.3 eV, which correspond to the C and O atoms. According to the method of gaussian peak fitting, the C1s and O1s curves are deconvoluted and fitted. The C1s high resolution XPS spectrum in Fig. 4f shows four peaks at 284.4, 285.3, 286.1 and 287.5 eV, which are related to chemical bond C=C, C-O-C, C-OH and C=O, respectively [21]. Similarly, the O1s high resolution XPS spectrum in Fig. 4g shows four peaks at 531.8, 532.6, 533.5 and 535.5 eV, which correspond to O-H, C-O, C=O and absorbed H_2O [38,39]. Hence, the XPS spectra also demonstrate the existence of rich oxygen-containing functional groups, which are in good agreement with the previous IR spectra.

3.3. Electrochemical analysis of the A-WRSC

The electrochemical property of activated carbon made from wild rice stem is studied in aqueous electrolyte with 6 M KOH. In three-electrode configuration, the A-WRSC is used as a working electrode, Hg/HgO as a reference electrode and Pt mesh as an auxiliary electrode. Fig. 5a shows the CV profiles of WRSC-800, A-WRSC-700, A-WRSC-800 and A-WRSC-900 electrodes at a scan rate of 100 mV/s in the potential range of -1-0 V. All the CV curves display quasi-rectangular shape, which typically represents an electrochemical double-layer capacitance behavior. Moreover, the A-WRSC-800 sample has the biggest curve integral area which indicates a superior capacitance. The CV curves of A-WRSC-800 at different scan rates are described in Fig. 5b. All the curves have a similar rectangular shape and exhibit good capacitance performance.

Subsequently, the GCD curves of WRSC-800, A-WRSC-700, A-WRSC-800 and A-WRSC-900 electrodes at the same current density of 1 A/g are measured and shown in Fig. 5c. Due to the presence of oxygen-containing functional groups in the carbon material, more electroactive sites are created for charge storage in the electrochemical process. So we observe triangular charging-discharging curves and higher capacitances. As can be seen from Fig. 5d, A-WRSC-800 displays graceful charging-discharging curves in current densities of 0.5–5 A/g. The specific capacitances of A-WRSC-800 at current densities of 0.5, 1, 2, 3, 4 and 5 A/g are 377, 301, 260, 252, 243 and 240 F/g, respectively (Fig. 5e). Table 1 lists the specific capacitances of carbon materials made from other biomass. It indicates that A-WRSC-800 exhibits higher specific capacitance than other bio-derived activated materials owing to its moderate microporous and mesoporous structures.

It is known to all that long cycle stability is one of the vital advantages of supercapacitors. We hence examine the cycling capability of A-WRSC-800 (Fig. 5f) at current density of 5 A/g. After 20000 cycles, 98% of the initial capacitance is still retained. It has better cycling stability than some other carbon materials [40,46].

In order to explore the practical application values of the A-WRSC-800, two identical electrodes made from A-WRSC-800 are assembled into a symmetric supercapacitor configuration using 6 M KOH aqueous electrolyte at the voltage range of 0–1 V. The CV curves of the two-electrode system are exhibited in Fig. 6a. They all show a nearly rectangular shape with humps, indicating the existence of both pseudocapacitance and electrical double layer capacitance. The constant current charge-discharge curves in Fig. 6b show good capacitive properties, from which the specific capacitances can be calculated. They are 94, 81, 75, 71, 65, 60, 49.5, 46.5, 44.5 and 32 F/g at current densities of 0.5, 1, 1.5, 2, 2.5, 3, 5, 10, 15 and 20 A/g, respectively (Fig. 6c). The good electrochemical performance results from the abundant microporous structure and surface functional groups [22,47]. Furthermore, the cycling stability is tested at current density of 5 A/g. The electrode still remains 87% of the initial capacitance after 10,000 cycles (Fig. 6d).

The Ragone plot of the symmetric supercapacitor is shown in Fig. 6e. The energy density gradually decreases as the increasing of the power density. The maximum energy density of 13.05 Wh/kg is

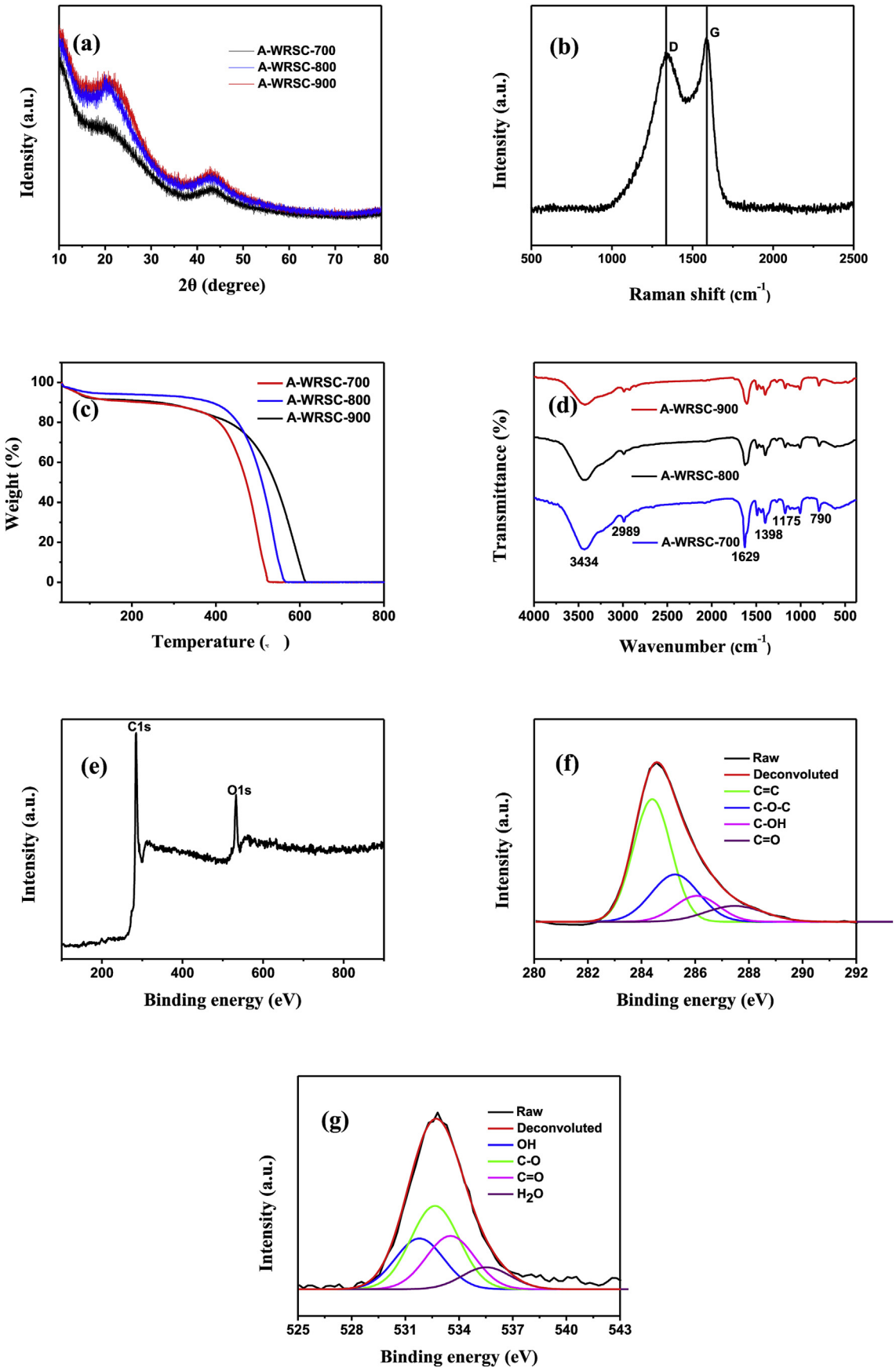

Fig. 4. XRD patterns (a), TGA profiles (c) and FT-IR spectra (d) of A-WRSC-700, A-WRSC-800 and A-WRSC-900; Raman spectra (b) and XPS survey spectra (e) of A-WRSC-800; C1s signal (f) and O1s signal (g) in XPS spectra of A-WRSC-800.

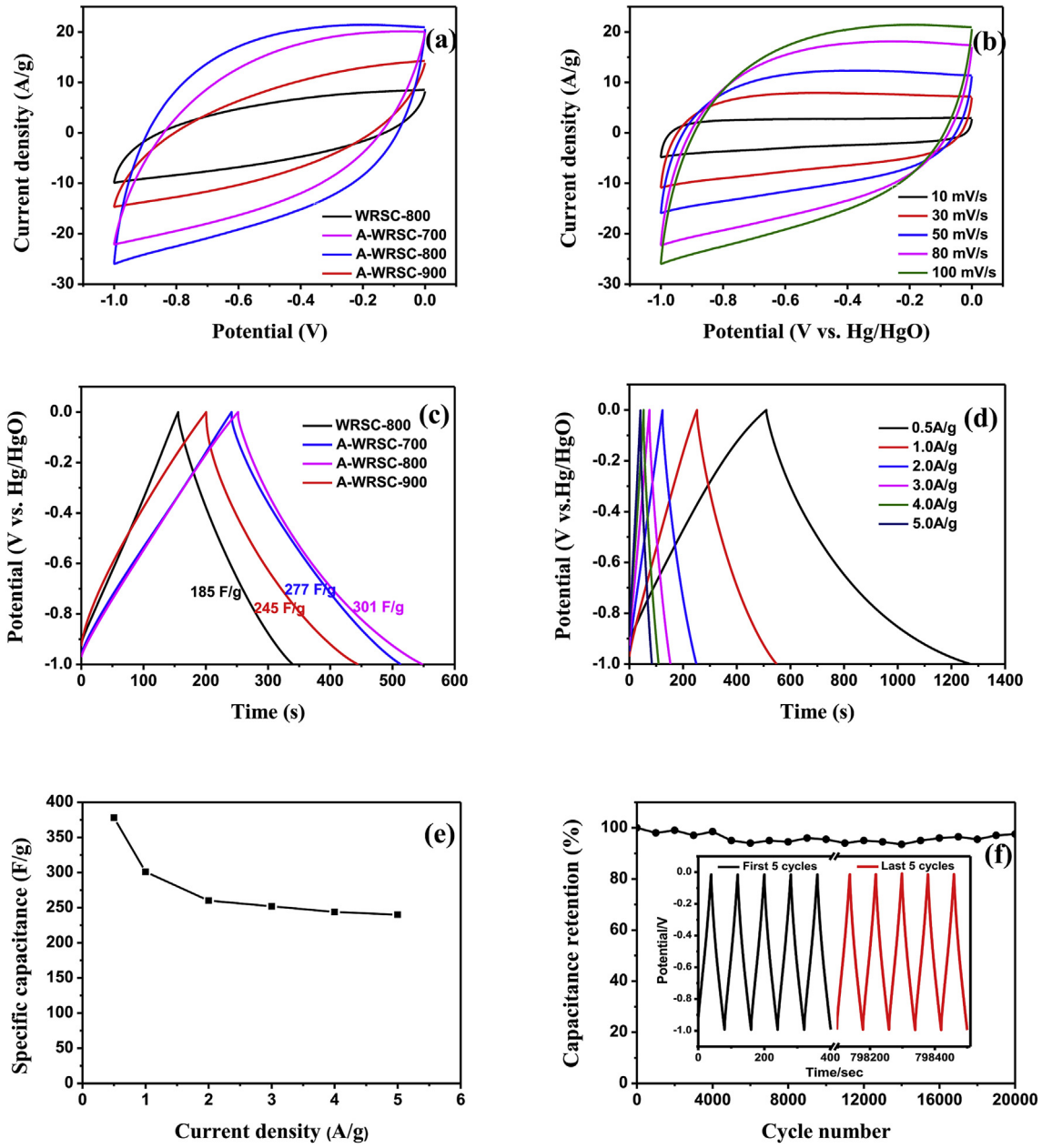

Fig. 5. CV curves of the WRSC-800, A-WRSC-700, A-WRSC-800 and A-WRSC-900 at 100 mV/s (a); CV curves of A-WRSC-800 at different scan rates (b); GCD curves of the WRSC-800, A-WRSC-700, A-WRSC-800 and A-WRSC-900 at 1 A g^{-1} (c); GCD curves (d) and specific capacitances (e) of the A-WRSC-800 at different current densities; Cycling stabilities (f) of A-WRSC-800 electrode at 5 A g^{-1}.

Table 1
Comparison of capacitances of bio-derived activated carbon materials.

Carbon sources	Specific capacitances (F/g)	Current density (A/g)	Electrolyte	References
Bamboo	301	0.1	6 M KOH	[18]
Banana peel	206	1.0	6 M KOH	[19]
Paulownia flower	297	1.0	6 M KOH	[21]
Almond shells	272.3	1.0	6 M KOH	[26]
Willow catkins	279	1.0	6 M KOH	[40]
Carrageenan	230	1.0	6 M KOH	[41]
Coconut shell	192	1.0	6 M KOH	[42]
Camellia oleifera	266	0.2	6 M KOH	[43]
Nori	220	0.1	6 M KOH	[44]
Scrap waste tires	106	1.0	6 M KOH	[45]
Wild rice stem	301	1.0	6 M KOH	This work

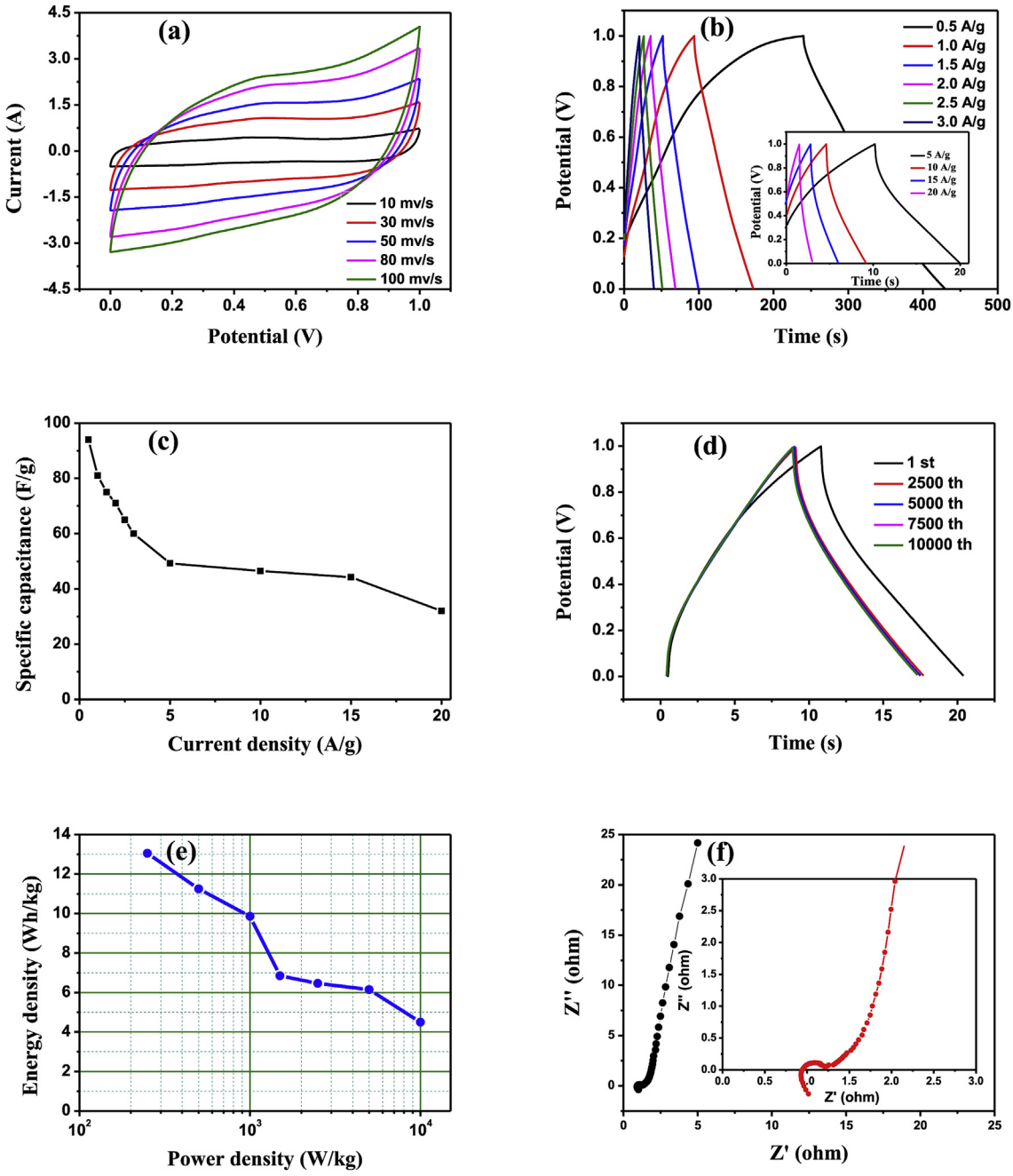

Fig. 6. CV (a) and GCD (b) curves of A-WRSC-800 electrode materials in symmetric supercapacitor with different scan rates and current densities, respectively; Specific capacitances (c) at different current densities and capacitance retention (d) after 5000 cycles; Ragone plot (e) of A-WRSC-800 electrode in symmetric supercapacitor at different current densities; Nyquist plots (f) of A-WRSC-800 supercapacitor.

achieved at the power density of 250 W/kg, which is superior to other reported carbon materials [17,18,48].

Electrochemical impedance is one of the important tools to present capacitance performance of the materials [49–52]. The Nyquist plot of A-WRSC-800 supercapacitor is shown in Fig. 6f. It mainly includes a semicircle and a straight line in high and low frequency region, respectively. In the Nyquist plot, the equivalent series resistance (Rs) is the intercept value between the semicircle and the X axis. The semicircular diameter value denotes the contact resistance (Rct), which represents the process of charge-transfer and reflects the device capacitance and electrochemical reaction behavior. The equivalent series resistance (Rs) and Rct of this supercapacitor are 0.95 Ω and 0.36 Ω, which indicates good rate capability and convenient contact between electrolyte ions and electrode materials [53,54]. In the low frequency region, straight line indicates the diffusion process of electrolyte ions. The high phase angle (about 80°) reflects a lower Warburg resistance. So electrolyte ions can rapidly enter into the material and show good electrical double layer capacitance behavior.

4. Conclusions

It is well established that characteristic of carbon electrodes, such as composition, crystal structure and morphological features,

and the sur-/interface properties between the electrode and electrolyte, greatly influence the performance of the carbon materials in electrochemical energy storage [55]. The present work for the first time demonstrates that the carbon material made from wild rice stem has bright prospects for application in supercapacitors. One of the activated carbons, A-WRSC-800, shows a high specific surface area of 1228 m^2/g because of rich microporous and mesoporous structures proved by BET analysis. The A-WRSC-800 displays a specific capacitance of 301 F/g at current density of 1 A/g in a three-electrode configuration. Furthermore, the assembled supercapacitor achieves the highest energy density of 13.05 Wh/kg at current density of 0.5 A/g. Thus, the carbon materials made from wild rice stem have extensive applications in supercapacitors.

Acknowledgments

This work was supported by the National Science Foundation of China (51573126).

References

[1] Z.S. Wu, G. Zhou, L.C. Yin, W. Ren, F. Li, H.M. Cheng, Graphene/metal oxide composite electrode materials for energy storage, Nano Energy 1 (2012) 107–131.
[2] L. Zolin, Jijeesh R. Nair, D. Beneventi, F. Bella, M. Destro, P. Jagdale, I. Cannavaro, A. Tagliaferro, D. Chaussy, F. Geobaldo, C. Gerbaldi, A simple route toward next-gen green energy storage concept by nanofibres-based self-supporting electrodes and a solid polymeric design, Carbon 107 (2016) 811–822.
[3] F. Bella, S. Galliano, M. Falco, G. Viscardi, C. Barolo, M. Grätzel, C. Gerbaldi, Approaching truly sustainable solar cells by the use of water and cellulose derivatives, Green Chem. 19 (2017) 1043–1051.
[4] F. Bella, D. Pugliese, L. Zolin, C. Gerbaldi, Paper-based quasi-solid dye-sensitized solar cells, Electrochim. Acta 237 (2017) 87–93.
[5] R.B. Rakhi, W. Chen, M.N. Hedhili, D. Cha, H.N. Alshareef, Enhanced rate performance of mesoporous Co3O4 nanosheet supercapacitor electrodes by hydrous RuO2 nanoparticle decoration, ACS Appl. Mater. Interfaces 6 (2014) 4196–4206.
[6] B. Qu, L. Hu, Q. Li, Y. Wang, L. Chen, T. Wang, High performance lithium ion battery anode by direct growth of hierarchical $ZnCo_2O_4$ nanostructures on current collectors, ACS Appl. Mater. Interfaces 6 (2014) 731–736.
[7] J.R. Miller, P. Simon, Electrochemical capacitors for energy management, Science 321 (2008) 651–652.
[8] M. Salanne, B. Rotenberg, K. Naoi, K. Kaneko, P.L. Taberna, C.P. Grey, B. Dunn, P. Simon, Efficient storage mechanisms for building better supercapacitors, Nature Energy 1 (2016) 16070–16079.
[9] H. Bi, T. Lin, F. Xu, Y. Tang, Z. Liu, F. Huang, New graphene form of nanoporous monolith for excellent energy storage, Nano Lett. 16 (2016) 349–354.
[10] P. Sharma, T.S. Bhatti, A review on electrochemical double-layer capacitors, Energ. Convers. Manage 51 (2010) 2901–2912.
[11] L.L. Zhang, X.S. Zhao, Carbon-based materials as supercapacitor electrodes, Chem. Soc. Rev. 38 (2009) 2520–2531.
[12] H. Chen, D. Liu, Z.H. Shen, B.F. Bao, S.Y. Zhao, L.M. Wu, Functional biomass carbons with hierarchical porous structure for supercapacitor electrode materials, Electrochim. Acta 180 (2015) 241–251.
[13] L.L. Wang, M.M. Jia, W.Q. Lu, K.L. Yang, J.Q. Fan, G. Liao, J.G. Yu, A facile route for preparation of high-performance hierarchical porous carbons for supercapacitor electrodes, Int. J. Electrochem. Sc 11 (2016) 6052–6063.
[14] Z.N. He, G.X. Zhang, Y.M. Chen, Y. Xie, T. Zhu, H.B. Guo, Y.G. Chen, The effect of activation methods on the electrochemical performance of ordered mesoporous carbon for supercapacitor applications, J. Mater. Sci. 52 (2017) 2422–2434.
[15] L.L. Ding, B. Zou, Y.N. Li, H.Q. Liu, Z.C. Wang, C. Zhao, Y. Su, Y.P. Guo, The production of hydrochar-based hierarchical porous carbons for use as electrochemical supercapacitor electrode materials, Colloid Surface A 423 (2013) 104–111.
[16] F. Barzegar, A. Bello, D. Momodu, M.J. Madito, J. Dangbegnon, N. Manyala, Preparation and characterization of porous carbon from expanded graphite for high energy density supercapacitor in aqueous electrolyte, J. Power Sources 309 (2016) 245–253.
[17] R. Mo, Y. Zhao, M. Wu, H. Xiao, S. Kuga, Y. Huang, J. Li, S. Fu, Activated carbon from nitrogen rich watermelon rind for high-performance supercapacitors, RSC Adv. 6 (2016) 59333–59342.
[18] W. Tian, Q. Gao, Y. Tan, K. Yang, L. Zhu, C. Yang, H. Zhang, Bio-inspired beehive-like hierarchical nanoporous carbon derived from bamboo-based industrial byproduct as a high performance supercapacitor electrode material, J. Mater. Chem. A 3 (2015) 5656–5664.
[19] Y. Lv, L. Gan, M. Liu, W. Xiong, Z. Xua, D. Zhu, D. Wright, A self-template synthesis of hierarchical porous carbon foams based on banana peel for supercapacitor electrodes, J. Power Sources 209 (2012) 152–157.
[20] S.T. Senthilkumar, R. Kalai Selvan, J.S. Melo, C. Sanjeeviraja, High performance solid-state electric double layer capacitor from redox mediated gel polymer electrolyte and renewable tamarind fruit shell derived porous carbon, ACS Appl. Mater. Interfaces 5 (2013) 10541–10550.
[21] J. Chang, Z. Gao, X. Wang, D. Wu, F. Xu, X. Wang, Y. Guo, K. Jiang, Activated porous carbon prepared from paulownia flower for high performance supercapacitor electrodes, Electrochim. Acta 157 (2015) 290–298.
[22] K.L. Sun, S.S. Yu, Z.L. Hu, Z.H. Li, G.T. Lei, Q.Z. Xiao, Y.H. Ding, Oxygen-containing hierarchically porous carbon materials derived from wild jujube pit for high-performance supercapacitor, Electrochim. Acta 231 (2017) 417–428.
[23] X. Xu, J. Gao, Q. Tian, X. Zhai, Y. Liu, Walnut shell derived porous carbon for a symmetric all-solid-state supercapacitor, Appl. Surf. Sci. 411 (2017) 170–176.
[24] N. Sudhan, K. Subramani, M. Karnan, N. Ilayaraja, M. Sathish, Biomass-derived activated porous carbon from rice straw for a high-energy symmetric supercapacitor in aqueous and non-aqueous electrolytes, Energy Fuels 31 (2017) 977–985.
[25] M. Karnan, K. Subramani, N. Sudhan, N. Ilayaraja, M. Sathish, Aloe vera derived activated high-surface-area carbon for flexible and high-energy supercapacitors, ACS Appl. Mater. Interfaces 8 (2016) 35191–35202.
[26] C. Wu, S.R. Yang, J.J. Cai, Q.B. Zhang, Y. Zhu, K.L. Zhang, Activated microporous carbon derived from almond shells for high energy density asymmetric supercapacitors, ACS Appl. Mater. Interfaces 8 (2016) 15288–15296.
[27] D. Momodu, M. Madito, F. Barzegar, A. Bello, A. Khaleed, O. Olaniyan, J. Dangbegnon, N. Manyala, Activated carbon derived from tree bark biomass with promising material properties for supercapacitors, J. Solid State Electr 21 (2017) 859–872.
[28] G. Hasegawa, M. Aoki, K. Kanamori, K. Nakanishi, T. Hanada, K. Tadanaga, Monolithic electrode for electric double-layer capacitors based on macro/meso/microporous S-containing activated carbon with high surface area, J. Mater. Chem. 21 (2011) 2060–2063.
[29] C. Wu, J. Gao, Q. Zhao, Y. Zhang, Y. Bai, X. Wang, X. Wang, Preparation and supercapacitive behaviors of the ordered mesoporous/microporous chromium carbide-derived carbons, J. Power Sources 269 (2014) 818–824.
[30] H. Chen, D. Liu, Z.H. Shen, B.F. Bao, S.Y. Zhao, L.M. Wu, Functional biomass carbons with hierarchical porous structure for supercapacitor electrode materials, Electrochim. Acta 180 (2015) 241–251.
[31] Y. Zhu, S. Murali, M.D. Stoller, K.J. Ganesh, W. Cai, P.J. Ferreira, A. Pirkle, R.M. Wallace, K.A. Cychosz, M. Thommes, D. Su, E.A. Stach, R.S. Ruoff, Carbon-based supercapacitors produced by activation of graphene, Science 332 (2011) 1537–1541.
[32] E. Raymundo-Pinero, P. Azais, T. Cacciaguerra, D. Cazorla-Amoros, A. Linares-Solano, F. Beguin, KOH and NaOH activation mechanisms of multiwalled carbon nanotubes with different structural organization, Carbon 43 (2005) 786–795.
[33] X. He, N. Zhao, J. Qiu, N. Xiao, M. Yu, C. Yu, M. Zheng, Synthesis of hierarchical porous carbons for supercapacitors from coal tar pitch with nano-Fe_2O_3 as template and activation agent coupled with KOH activation, J. Mater. Chem. A 1 (2013) 9440–9448.
[34] W. Qian, F. Sun, Y. Xu, L. Qiu, C. Liu, S. Wan, F. Yan, Human hair-derived carbon flakes for electrochemical supercapacitors, Energy Environ. Sci. 7 (2014) 379–386.
[35] W.M. Lv, F.S. Wen, J.Y. Xiang, J. Zhao, L. Li, L.M. Wang, Z.Y. Liu, Y.J. Tian, Peanut shell derived hard carbon as ultralong cycling anodes for lithium and sodium batteries, Electrochim. Acta 176 (2015) 533–541.
[36] P. Dhanya, V. Aravindan, M. Srinivasan, S. Ogale, 3D micro-porous conducting carbon beehive by single step polymer carbonization for high performance supercapacitors: the magic of in situ porogen formation, Energy Environ. Sci. 7 (2014) 728–735.
[37] D. Hulicova-Jurcakova, M. Seredych, G.Q. Lu, T.J. Bandosz, Combined effect of nitrogen- and oxygen-containing functional groups of microporous activated carbon on its electrochemical performance in supercapacitors, Adv. Funct. Mater. 19 (2009) 438–447.
[38] Y.Y. Wang, B.H. Hou, H.Y. Lü, C.L. Lü, X.L. Wu, Hierarchically porous N-doped carbon nanosheets derived from grapefruit peels for high-performance supercapacitors, ChemistrySelect 1 (2016) 1441–1447.
[39] Y. Zhao, W. Ran, J. He, Y. Song, C. Zhang, D.B. Xiong, F. Gao, J. Wu, Y. Xia, Oxygen-rich hierarchical porous carbon derived from artemia cyst Shells with superior electrochemical performance, ACS Appl. Mater. Interfaces 7 (2015) 1132–1139.
[40] K. Wang, N. Zhao, S. Lei, R. Yan, X. Tian, J. Wang, Y. Song, D. Xu, Q. Guo, L. Liu, Promising biomass-based activated carbons derived from willow catkins for high performance supercapacitors, Electrochim. Acta 166 (2015) 1–11.
[41] Y. Fan, X. Yang, B. Zhu, P.F. Liu, H.T. Lu, Micro-mesoporous carbon spheres derived from carrageenan as electrode material for supercapacitors, J. Power Sources 268 (2014) 584–590.
[42] J. Mi, X.R. Wang, R.J. Fan, W.H. Qu, W.C. Li, Coconut-shell-based porous carbons with a tunable micro/mesopore ratio for high-performance supercapacitors, Energy Fuels 26 (2012) 5321–5329.
[43] J. Zhang, L. Gong, K. Sun, J. Jiang, X. Zhang, Preparation of activated carbon from waste Camellia oleifera shell for supercapacitor application, J. Solid State Electrochem. 16 (2012) 2179–2186.
[44] C.S. Wang, T.Z. Liu, Nori-based N, O, S, Cl co-doped carbon materials by chemical activation of $ZnCl_2$ for supercapacitor, J. Alloy. Comp. 696 (2017)

42–50.
[45] M.J. Zhi, F. Yang, F.K. Meng, M.Q. Li, A. Manivannan, N.Q. Wu, Effects of pore structure on performance of an activated-carbon supercapacitor electrode recycled from scrap waste tires, ACS Sustain. Chem. Eng. 2 (2014) 1592–1598.
[46] J. Zhang, L. Gong, K. Sun, J. Jiang, X. Zhang, Preparation of activated carbon from waste camellia oleifera shell for supercapacitor application, J. Solid State Electr 16 (2012) 2179–2186.
[47] V. Khairnar, T. Soga, M. Sharon, S. Jaybhaye, C.C. Hu, R. Afre, M. Sharon, Development of supercapacitors using porous carbon materials synthesized from plant derived precursors, Carbon Lett. 9 (2008) 188–189.
[48] Q. Xie, R. Bao, A. Zheng, Y. Zhang, S. Wu, C. Xie, P. Zhao, Sustainable low-cost green electrodes with high volumetric capacitance for aqueous symmetric supercapacitors with high energy density, ACS Sustain. Chem. Eng. 4 (2016) 1422–1430.
[49] E. Frackowiak, F. Béguin, Carbon materials for the electrochemical storage of energy in capacitors, Carbon 39 (2001) 937–950.
[50] M.K. Rofouei, H. Khoshsafar, R.J. Kalbasi, H. Bagheri, A sensitive electrochemical sensor for the determination of carvedilol based on a modified glassy carbon electrode with ordered mesoporous carbon, RSC Adv. 6 (2016) 13160–13167.
[51] H. Bagheri, A. Afkhami, H. Khoshsafar, M. Rezaei, S.J. Sabounchei, M. Sarlakifar, Simultaneous electrochemical sensing of thallium, lead and mercury using a novel ionic liquid/graphene modified electrode, Anal. Chim. Acta 870 (2015) 56–66.
[52] P. Hashemi, H. Bagheri, A. Afkhami, Y.H. Ardakani, T. Madrakian, Fabrication of a novel aptasensor based on three-dimensional reduced graphene oxide/polyaniline/gold nanoparticle composite as a novel platform for high sensitive and specific cocaine detection, Anal. Chim. Acta 996 (2017) 10–19.
[53] B.G. Choi, M. Yang, W.H. Hong, J.W. Choi, Y.S. Huh, 3D macroporous graphene frameworks for supercapacitors with high energy and power densities, ACS Nano 6 (2012) 4020–4028.
[54] Z. Lei, Z. Liu, H. Wang, X. Sun, L. Lu, X. Zhao, A high-energy-density supercapacitor with graphene–CMK-5 as the electrode and ionic liquid as the electrolyte, J. Mater. Chem. A 1 (2013) 2313–2321.
[55] L. Wei, M. Sevilla, A.B. Fuertes, R. Mokaya, G. Yushin, Hydrothermal carbonization of abundant renewable natural organic chemicals for high-performance supercapacitor electrodes, Adv. Energy Mater 1 (2011) 356–361.